



# Measurement and Analysis of Radar-Cross-Section of UAV at 21–26 GHz Frequency Band

AN Hao<sup>1</sup>, LIU Ting<sup>1</sup>, HE Danping<sup>1</sup>, MA Yihua<sup>2</sup>, DOU Jianwu<sup>2</sup>

(1. State Key Laboratory of Advanced Rail Autonomous Operation, Beijing Jiaotong University, Beijing 100044, China;

2. State Key Laboratory of Mobile Network and Mobile Multimedia Technology, ZTE Corporation, Shenzhen 518057, China)

DOI: 10.12142/ZTECOM.202501014

<https://kns.cnki.net/kcms/detail/34.1294.TN.20250210.1609.002.html>,  
published online February 11, 2025

Manuscript received: 2023–10–11

**Abstract:** With the emergence of the 6G technology, integrated sensing and communication (ISAC) has become a hot-spot vertical application. The low-altitude scenario is considered to be a significant use case of the ISAC. However, the existing channel model is hard to meet the demands of the sensing function. The radar-cross-section (RCS) is a critical feature for the sensing part, while accurate RCS data for the typical frequency band of ISAC are still lacking. Therefore, this paper conducts measurements and analysis of the RCS data of the unmanned aerial vehicles (UAVs) under multiple poses and angles in real flying conditions. The echo from a UAV is acquired in an anechoic chamber, and the RCS values are calculated. The results of different flying attitudes are analyzed, providing RCS features for the ISAC applications.

**Keywords:** unmanned aerial vehicle; radar-cross-section; integrated sensing and communication; anechoic chamber measurement

**Citation** (Format 1): AN H, LIU T, HE D P, et al. Measurement and analysis of radar-cross-section of UAV at 21 – 26 GHz frequency band [J]. *ZTE Communications*, 2025, 23(1): 107 – 114. DOI: 10.12142/ZTECOM.202501014

**Citation** (Format 2): H. An, T. Liu, D. P. He, et al., “Measurement and analysis of radar-cross-section of UAV at 21 – 26 GHz frequency band,” *ZTE Communications*, vol. 23, no. 1, pp. 107 – 114, Mar. 2025. doi: 10.12142/ZTECOM.202501014.

## 1 Introduction

With the development of 6G, the integrated sensing and communication (ISAC) process is accelerating. An essential scenario for ISAC is the low-altitude environment, which includes specific use cases such as trunking communication and ad-hoc networks. Research on channel modeling for ISAC is now under lively discussion. However, the topic is mainly on the intelligent connected vehicles<sup>[1]</sup>, and channel modeling for the low-altitude scenario with unmanned aerial vehicles (UAVs) as protagonists still needs to be further explored. The communications, sensing, and computing resources will be deeply integrated and mutually beneficial, providing efficient services for new intelligent applications such as intelligent transportation, UAV networks, space-air-ground-sea integrated networks, environmental detection, and metaverse<sup>[2–3]</sup>. The application potential of the low-altitude scenario is significant, as networks of UAVs can be used as sensor platforms to enable remote location coverage in emergencies like network impairment. Alternatively, UAVs can be used as low-cost infrastructure to provide traffic offload in crowded areas like stadiums<sup>[4]</sup>. More-

over, applying UAV networks to high-speed railways, especially in high-altitude unmanned areas, will effectively reduce maintenance costs. Due to their high mobility and low cost, UAVs play an increasingly significant role in many practical applications, including weather monitoring, forest fire detection, and emergency search and rescue<sup>[5]</sup>. By building a collaborative network architecture with multiple air base stations, it is possible to achieve multi-service, multi-access, multi-level coverage for post-disaster scenarios<sup>[6]</sup>. Besides, UAVs are expected to serve as an efficient complementary to terrestrial wireless communication systems to provide enhanced coverage and reliable connectivity to ground users<sup>[7]</sup>. UAVs facilitate more advanced technologies, such as federated learning<sup>[8]</sup>, reconfigurable intelligent surface<sup>[9]</sup>, and the Internet of Things<sup>[10]</sup>. Mobile edge computing (MEC) has developed into a promising computing paradigm. UAVs are practical in MEC since federated learning can improve the performance of UAV computing networks<sup>[11]</sup>. While there are ample application prospects and advantages, UAVs face significant challenges. Due to the high mobility, the requirements for dynamic channel modeling are demanding<sup>[12]</sup>. The channel status changes rapidly and should be updated frequently. Therefore, conducting the underlying theory and critical technology study for the UAV channels is of great importance and value.

This work was supported by ZTE Industry-University-Institute Cooperation Funds under Grant No. HC-CN-20220622006.

More research efforts have been put into current UAV channel modeling. Ref. [13] performs a channel replication of a 1 420 MHz air-to-air link using ray tracing and tapped-delay line models to describe the communication channel. The low detectability of radar targets is crucial for stealth. To avoid being detected by radar, the reduction technology of radar-cross-section (RCS) has become one of the research hotspots<sup>[14]</sup>. Currently, there is some literature on RCS measurement and analysis of UAVs. Most studies are mainly focused on the X-band (8 – 12 GHz) radars and even lower frequency bands. Ref. [15] discusses the relationship between RCS and the UAV flight range through dynamic measurements by a radar demonstrator system at 8.75 GHz. Ref. [16] presents the results of the measurement and analysis of several UAV RCS in different planes and from different elevation angles at 9 GHz. Ref. [17] describes the measurement and modeling of the dynamic RCS at 8 – 10 GHz and compares the difference between the probability of detection using dynamic and static RCSes. Due to the development of wireless communication frequency bands towards higher frequencies such as millimeter-wave, terahertz, and visible light bands, there will be more and more overlap with traditional sensing frequency bands. Besides, there is a lack of data support for sensory characteristics in the typical ISAC frequency band. RCS-based measurements at 15 GHz and 25 GHz are used for UAV recognition and detection in Refs. [18] and [19]. Diverse UAV detection and classification methods based on the RCS signatures are analyzed at 26 – 40 GHz<sup>[20–21]</sup>. However, accurate data on the UAVs for the ISAC frequency band is far from enough. It is worth noting that the structure and materials of the UAVs are different. Thus, the RCS values cannot be represented by a unified model. In addition, considering the variable attitude of the UAVs during flight and the unfixed relative positions between the UAVs and the base stations, conducting RCS measurements in practical scenarios is also challenging. Therefore, conducting multiple measurements and analyzing RCS values for different propeller states and attitudes while the UAV is stationary may be the most feasible approach. Channel models for communication functions can provide large- and small-scale channel parameters, while the contribution to sensing is weak. The sensing feature needs to be modeled accurately since the sensing function is considered a fundamental function of 6G networks. Collaborative perception can be achieved by deploying multiple UAVs<sup>[22]</sup>. From the existing literature, changes in the UAV structures have not attracted much attention. During the flight, the propeller states and attitudes are variable, which is also crucial for sensing. Therefore, accurate RCS data for the UAV structure changes at the key frequency band for communication sensing, i.e., 21 – 26 GHz, are essential and need to be further supplemented.

In response to the abovementioned demands and challenges, measurements are carried out for a typical UAV in this paper. Multi-angle bistatic measurements are conducted at dif-

ferent flight attitudes of 21 – 26 GHz. Accurate multi-angle RCSs are obtained after calibration and statistical analyses were performed. This study provides a data basis for the UAV application of ISAC and complements the missing measurement data of multiple attitudes and angles of UAVs in this frequency range. Besides, this work will contribute to the development of accurate ray-tracing simulation models for UAV scenarios<sup>[23–24]</sup>, providing essential data support for ISAC channel standardization. The main contributions and novelties of this paper are as follows.

- An RCS measurement system is built based on a vector network analyzer (VNA) and a rotary table, which can measure the RCS and maximum received power of the UAV at any angle;
- The measurement data of RCS for quadcopter drones in the 21 – 26 GHz frequency band are filled;
- The RCS of the UAV in different flight attitudes, propeller states, and angles between the transmitting and receiving antennas are measured, and the effects are compared.

The rest of this paper is organized as follows. Section 2 describes the RCS measurement system and layouts. The measurement results are introduced in Section 3, including the reference data, maximum received power, and RCS. Conclusions are drawn in Section 4.

## 2 Measurement Campaign

### 2.1 Measurement System

The RCS measurement of a UAV is carried out in an anechoic chamber to reduce the interference of external electromagnetic wave signals. At the same time, the absorbing materials reduce the multipath effects caused by the reflection of walls and ceilings. The measurement system consists of a VNA, a rotary table, two identical directional antennas, two tripods, and a quadcopter UAV, as shown in Fig. 1. The rotary table is made of low-density foam material, and its influence on electromagnetic wave propagation can be ignored. The UAV is placed on the rotary table and rotates synchronously with it.

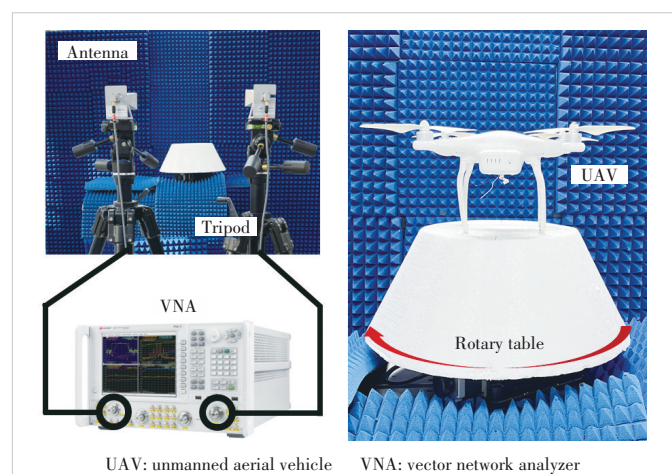


Figure 1. Proposed measurement system

The measurements are conducted at the center frequency of 23.5 GHz with a 5 GHz bandwidth. The frequency sampling number is 201, which indicates a frequency sampling resolution of 25 MHz. The gain of both directional antennas is 24.7 dBi to enhance the received signal strength. During the measurement process, the transceiver antenna is fixed on a tripod, and the UAV is placed on the rotary table to maintain the same antenna height. The heights of the Tx and the Rx from the ground are both 1.3 m, as well as the height of the UAV. The antennas and the UAV are at the same level to ensure that the antenna beams can cover the UAV. The rotary table is rotated at an interval of  $5^\circ$  during the measurements in order to measure the RCS at different angles as much as possible. The angles between the Tx and Rx are considered to be  $10^\circ$  and  $45^\circ$ . This is for comparing the RCS differences under different angles. More detailed measurement parameters are listed in Table 1.

## 2.2 UAV and Antenna Layouts

The UAV in the measurement is Phantom 3 Standard, which is one of the common camera drones. The diagonal size (propellers excluded) is 0.35 m. The length and width of the UAV are 0.25 m, and the height is 0.19 m.

Due to the difficulty of hovering the UAV, static measurements are carried out. To obtain the reflection and scattering characteristics of the various attitudes of the UAV, the fuselage states of leveling and tilting are considered. Besides, the propeller states of vertical and parallel to the aircraft axis are also considered. Thus, there are four types of UAV attitudes in the measurements in total, which are shown in Fig. 2a. Fig. 2b shows the positional relationship between the antennas and the UAV. All cases are summarized in Table 2. The distance between Tx and the UAV is 1.8 m. The distance between the UAV and Rx is 1.8 m. The diameters of the aircraft axes are

**Table 1. Measurement configuration**

Measurement Parameters	Values
Center frequency	23.5 GHz
Bandwidth	5.0 GHz
Frequency samples	201.0
Rotation angle interval	$5.0^\circ$
Tx and Rx heights from the ground	1.3 m
UAV height from the ground	1.3 m
Antenna gain	24.7 dBi
Angle between Tx and Rx	$10.0^\circ/45.0^\circ$

UAV: unmanned aerial vehicle

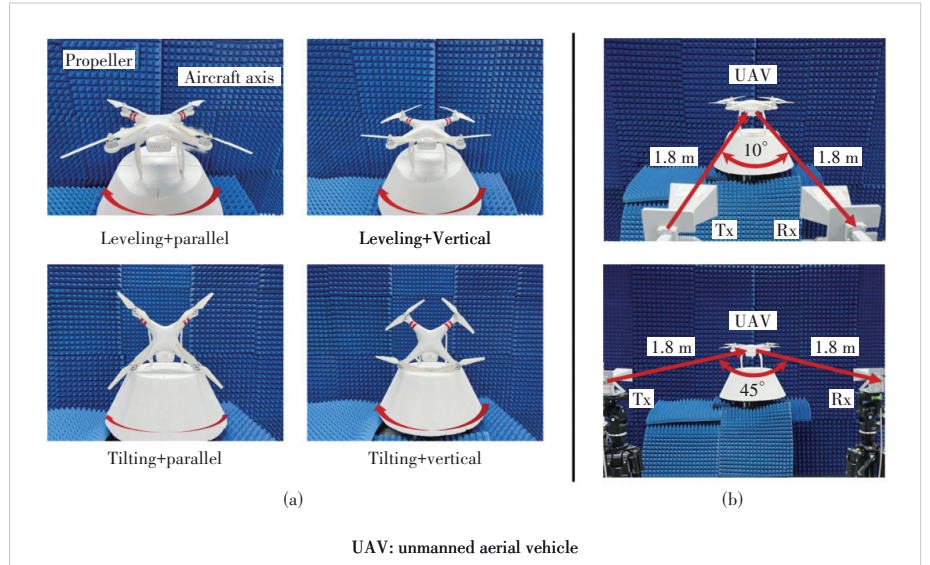


**Figure 2. Layout of the antennas and the UAV:(a) attitudes of the UAV and (b) the positional relationship between the antennas and the UAV**

**Table 2. Measurement cases**

Case	UAV States	Propeller States to Aircraft Axis	Angle Between Tx and Rx
1	Leveling	Parallel	$10^\circ$
2	Leveling	Vertical	
3	Tilting	Parallel	
4	Tilting	Vertical	
5	Leveling	Parallel	$45^\circ$
6	Leveling	Vertical	
7	Tilting	Parallel	
8	Tilting	Vertical	

UAV: unmanned aerial vehicle

0.03 m. The measurement meets the far-field conditions, according to the following equation:

$$d_f = 2D^2/\lambda \quad (1),$$

where  $d_f$  is the distance of the Fraunhofer region,  $D$  is the maximum linear dimension of the antenna, and  $\lambda$  is the wavelength.

## 3 Measurement Results

### 3.1 Reference Data

To obtain accurate antenna gains, measurements are conducted under line of sight (LoS) conditions. Besides, the case without placing the UAV is measured to provide a reference. The distance between the Tx and Rx is 3.6 m, which is twice the distance from the Tx or Rx to the UAV in the RCS measurements. Moreover, the power delay profiles (PDPs) with and without the UAV are compared, which is shown in Fig. 3.

Fig. 3 shows that the delays corresponding to the strongest power are the same in all cases. The power is the highest at

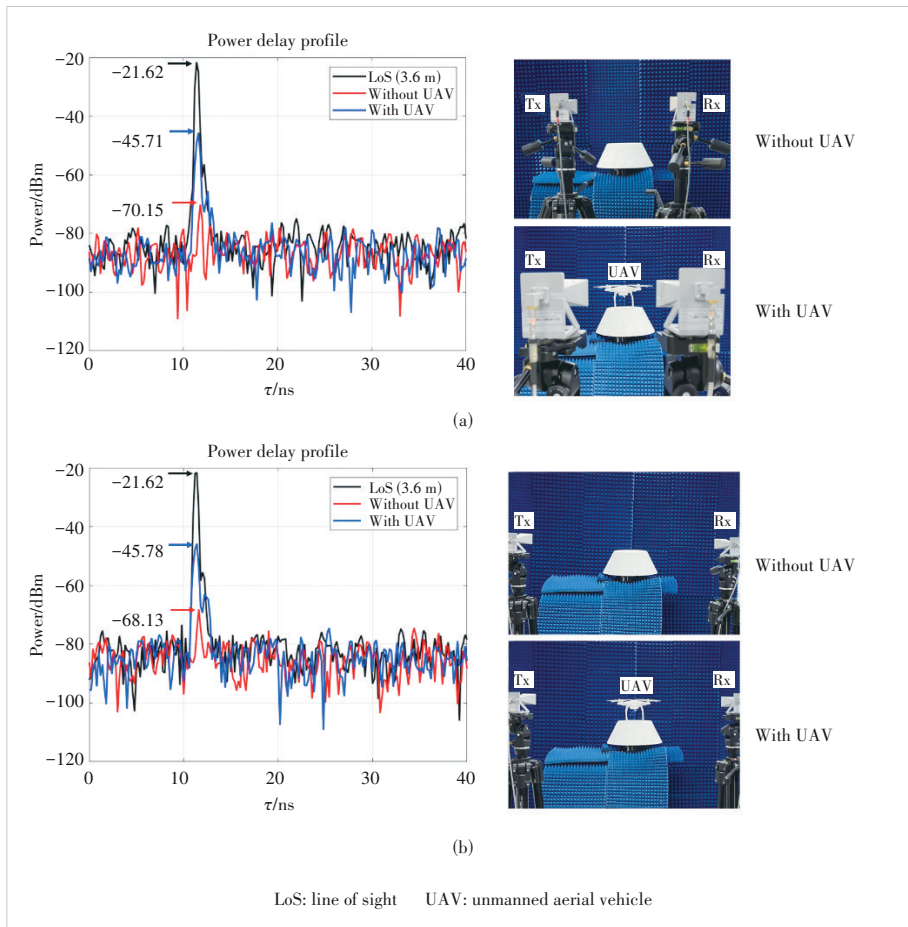


Figure 3. PDP comparison of the LoS and w/o the UAV at the Tx-Rx angle of (a) 10° and (b) 45°

the LoS and the lowest when there is no UAV placed, which indicates that the absorbing materials are very effective. Since Tx and Rx are the same, the antenna gain  $G_{\text{Ant}}$  can be calculated by:

$$G_{\text{Ant}} = (P_{\text{max}} + \text{FSPL}_{23.5 \text{ GHz}, 3.6 \text{ m}}) / 2 \quad (2)$$

where  $P_{\text{max}}$  denotes the maximum power of the PDP and  $\text{FSPL}_{23.5 \text{ GHz}, 3.6 \text{ m}}$  denotes the free space path loss at 3.6 m at the frequency of 23.5 GHz.

### 3.2 Maximum Received Power

The maximum power at each measurement angle is analyzed before RCS, which can help us gain a preliminary understanding of the reflection characteristics of the UAV at different angles. For each attitude of the UAV at two angles, the measurements are conducted every 5° of the rotation of the rotary table, and thus 72 measurement results are obtained. The values of the maximum power are found from all measured angles. The radar charts are shown in Fig. 4, where the maximum power is higher at the four measured angles of 0°, 90°, 180°, and 270°, which is mainly caused by the reflection of the battery module below the UAV. The power at the same

measurement angle varies slightly at different attitudes. In addition, the maximum power of Tx and Rx at the angle of 10° is generally higher than that at the angle of 45°.

### 3.3 RCS

The radar acquires the target information by processing the echo data. Therefore, the design and operation of radars are critical to quantify and describe the echo, especially in terms of target characteristics such as the size, shape, and orientation. For that purpose, the target is ascribed to an effective area called the RCS<sup>[25]</sup>. The RCS of the target is the ratio of the power scattered back to the radar receiver over the incident radar power density per unit of solid angles on the target, which is expressed as follows<sup>[26]</sup>:

$$\sigma = \frac{P_r (4\pi)^3 d_i^2 d_r^2}{P_t G_t G_r \lambda^2} \quad (3)$$

where  $\sigma$  represents the RCS,  $P_t$  and  $P_r$  represent the transmitted power and received power,  $d_i$  and  $d_r$  represent the distance from the target to Tx and Rx, and  $G_t$  and  $G_r$  represent the gain of Tx and Rx. Fig. 5 shows the RCS results

and cumulative distribution function (CDF) at each measured angle in the cases of two different angles between Tx and Rx. All the results are summarized in Table 3.

#### 1) Case 1

When the angle between the Tx and Rx is 10°, the UAV is leveling, and the propellers are parallel to the aircraft axis. The maximum value of RCS is obtained at 0° of the rotation in this condition, where the UAV faces the antennas. The battery module below the UAV generates a strong echo. The CDF shows that the mean value of the RCS in this case is about -31.68 dBsm.

#### 2) Case 2

When propellers are vertical to the aircraft axis, the maximum value of RCS is also obtained at 0° of the rotation. Compared with the previous UAV attitude scenario, values of the RCS are slightly different from those at the measured angles of 0°, 90°, 180°, and 270°. However, there are significant differences in other measured angles. Because, at those angles, the propellers are in the lobes of the Tx and Rx, significantly impacting the echo. From the CDF, the mean value of RCS in this case is also about -31.63 dBsm.

#### 3) Case 3

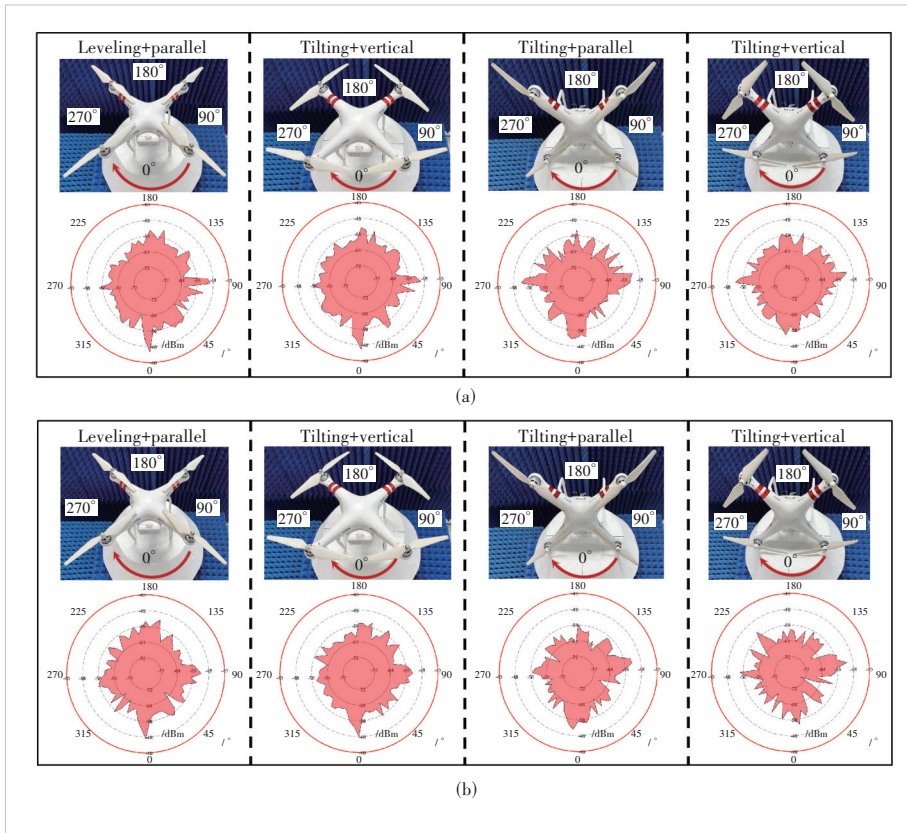


**Figure 4.** Maximum power at different attitudes at the Tx-Rx angles of (a)  $10^\circ$  and (b)  $45^\circ$

When the angle between the Tx and Rx is still  $10^\circ$ , the UAV changes to tilt, and the propellers are parallel to the aircraft axis. Like the previous ones, the maximum value of the RCS is also obtained at  $0^\circ$ , indicating that the reflecting surface on the top of the UAV still plays a crucial role. However, this value

**Table 3.** RCS measurement results

Case	RCS		
	Maximum Value/dBsm (Corresponding Angle)	Minimum Value/dBsm (Corresponding Angle)	Mean Value/ dBsm
1	-19.01 ( $0^\circ$ )	-38.81 ( $225^\circ$ )	-31.68
2	-19.40 ( $0^\circ$ )	-36.53 ( $45^\circ$ )	-31.63
3	-25.12 ( $350^\circ$ )	-40.87 ( $215^\circ$ )	-33.27
4	-24.72 ( $100^\circ$ )	-39.50 ( $290^\circ$ )	-32.85
5	-20.78 ( $0^\circ$ )	-40.33 ( $45^\circ$ )	-32.09
6	-21.78 ( $0^\circ$ )	-36.95 ( $255^\circ$ )	-32.36
7	-24.71 ( $355^\circ$ )	-42.93 ( $240^\circ$ )	-34.02
8	-24.59 ( $100^\circ$ )	-47.95 ( $65^\circ$ )	-34.63

RCS: radar-cross-section

significantly decreases as the size of the reflection surface in this case is smaller than that of the leveling ones. Besides, the values of the RCS fluctuate more sharply at other measured angles because of the UAV structure. Significant differences in the structure of the UAV at different angles lead to rapid changes in the size and shape of the reflecting surfaces. The mean value of the RCS in this case is about  $-33.27$  dBsm.

#### 4) Case 4

As for the case of the propellers being vertical to the aircraft axis, the maximum value of RCS is obtained at the measured angle of  $90^\circ$ . The rotation of the propellers affects the size of the reflecting surface. Compared with the case where the UAV is leveling and the propellers are vertical, the value of the RCS significantly decreases at  $0^\circ$ . Meanwhile, the values fluctuate more sharply at other measurement angles for the same reason as the previous one. The mean value of the RCS is about  $-32.85$  dBsm according to the CDF.

#### 5) Case 5

Fig. 5b shows the results of the RCS when the angle between the Tx and Rx is  $45^\circ$ . The maximum value of RCS is obtained at  $0^\circ$  while the UAV is leveling and the propellers are parallel to the aircraft axis. The RCS values at most measured angles slightly increase compared with those at  $10^\circ$ , given the same attitude, indicating that the reflection area is larger at this angle. The mean value of the RCS of the UAV in this case is about  $-32.09$  dBsm.

#### 6) Case 6

A similar situation occurs when the UAV is tilting and the propellers are vertical to the aircraft axis. The maximum value of the RCS is also obtained at  $0^\circ$ . Moreover, the mean value of the RCS is  $-32.36$  dBsm.

#### 7) Case 7

When the angle between the Tx and Rx is  $45^\circ$ , the UAV tilts and the propellers are parallel to the aircraft axis, and the maximum value of the RCS is also obtained at  $0^\circ$ . Besides, the values of the RCS show little change in most measured angles. The values of the RCS are mainly smaller than the case of the UAV leveling and the propellers are parallel to the aircraft axis in most measured angles because of the significant impact on the reflection surface. According to the CDF, the mean value of the RCS in this case is about  $-34.02$  dBsm.

#### 8) Case 8

As the UAV is tilting and the propellers are vertical to

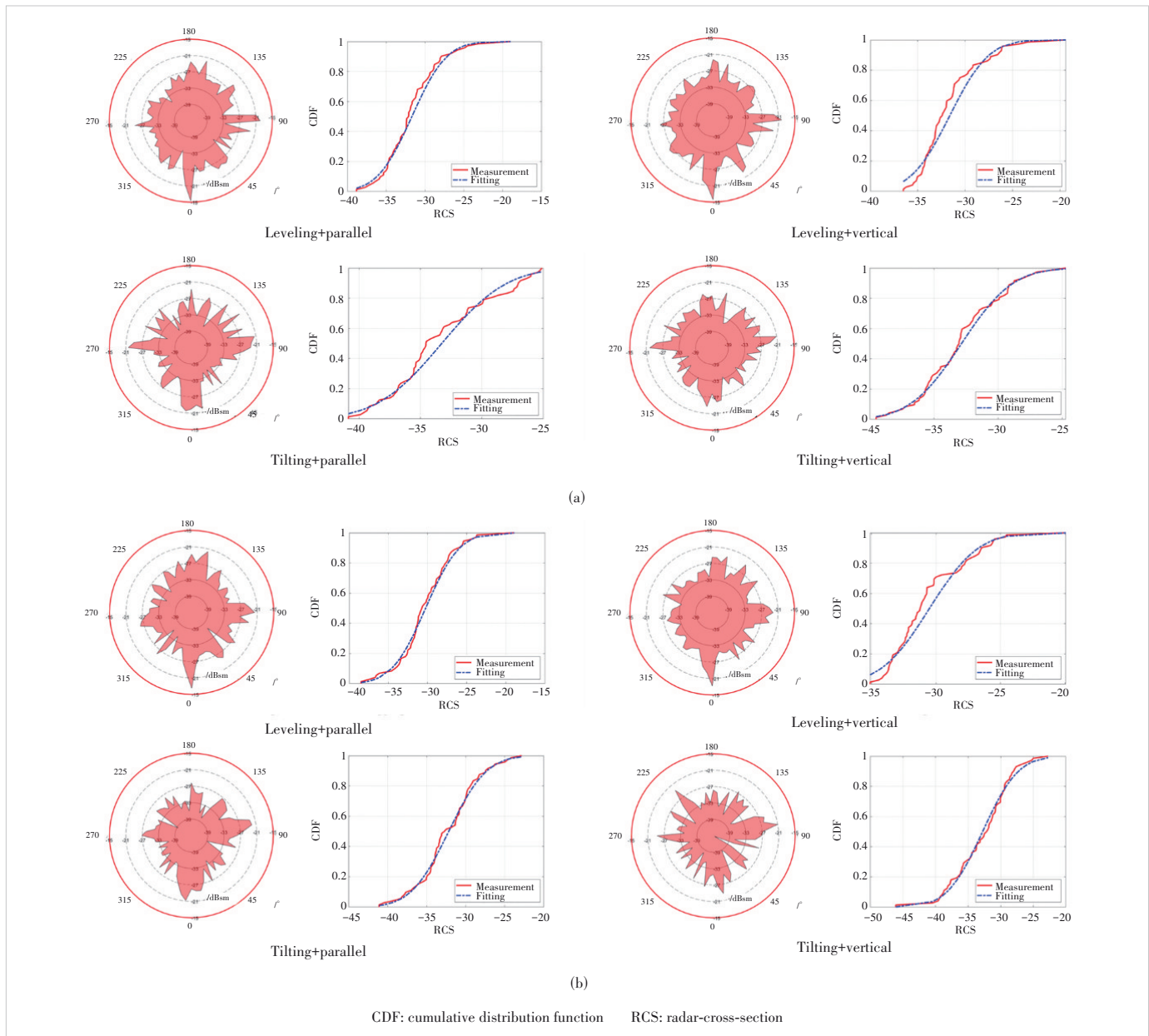


Figure 5. RCS of the UAV at different attitudes at the Tx-Rx angles of (a) 10° and (b) 45°

the aircraft axis, the maximum value of RCS is obtained at 90°, same with the situation when the angle between the Tx and Rx is 10°. However, the values of RCS show little difference from the situation where the angle between the Tx and Rx is 10° in most measured angles. Compared with the case of the UAV leveling and the propellers being vertical to the aircraft axis at the same angle between the Tx and Rx, most values of the RCS decrease as the tilt of the UAV at this angle causes a more significant impact on the reflection surface. Furthermore, the mean value of the RCS of the UAV is about -34.63 dBsm in this case.

### 4 Conclusions

In this paper, the UAV RCS measurements are conducted based on the VNA. The UAV is measured in all directions by using the rotary table. The angles between the Tx and Rx include 10° and 45°. Four types of UAV attitudes are considered for a comprehensive analysis. The UAV is leveling and tilting, and the propellers are parallel and vertical to the aircraft axis.

As for the measurement results, the maximum received power and the RCS are analyzed. For complex targets like UAVs, there is no fixed calculation relationship between their fuselage structure and RCS. It is found that the maximum

power is mainly affected by the reflection of the main part of the UAV rather than the attitudes. The power at the same measurement angle varies slightly at different attitudes. The angle between the Tx and Rx can also influence the results, with a smaller angle resulting in a higher maximum power. The maximum value of the RCS is mostly measured at around  $0^\circ$ , except for the case where the UAV is tilting and the propellers are vertical to the aircraft axis, which is obtained at  $100^\circ$ . The mean values of the RCS in different cases are between  $-31$  dBsm and  $-35$  dBsm. As the angle between the Tx and Rx increases, the values of RCS generally decrease. In addition, the attitude change will significantly impact the changes in the values of the RCS at different measured angles.

This paper provides reference data at the millimeter wave band for studying the ISAC channel of UAVs. The flight status of UAVs may be determined by constantly detecting RCS values. In addition, the results of this paper can also be used as data references for the ray-tracing simulation of UAVs<sup>[27]</sup>. Using the same method, more comprehensive measurements of multiple types of unmanned aerial vehicles, multiple frequency bands, and multiple flight attitudes can be conducted. The RCS models of different UAVs at different attitudes and incident angles can be explored in the future.

## References

- [1] CHENG X, DUAN D L, GAO S J, et al. Integrated sensing and communications (ISAC) for vehicular communication networks (VCN) [J]. *IEEE Internet of Things journal*, 2022, 9(23): 23441 – 23451. DOI: 10.1109/JIOT.2022.3191386
- [2] WANG C X, YOU X H, GAO X Q, et al. On the road to 6G: visions, requirements, key technologies, and testbeds [J]. *IEEE communications surveys & tutorials*, 2023, 25(2): 905 – 974. DOI: 10.1109/COMST.2023.3249835
- [3] WU H C, LI H J, TAO X F. Green air-ground integrated heterogeneous network in 6G era [J]. *ZTE communications*, 2021, 19(1): 39 – 47. DOI: 10.12142/ZTECOM.202101006
- [4] ALZHRANI B, OUBBATI O S, BARNAWI A, et al. UAV assistance paradigm: state-of-the-art in applications and challenges [J]. *Journal of network and computer applications*, 2020, 166: 102706. DOI: 10.1016/j.jnca.2020.102706
- [5] ZENG Y, ZHANG R, LIM T J. Wireless communications with unmanned aerial vehicles: opportunities and challenges [J]. *IEEE communications magazine*, 2016, 54(5): 36 – 42. DOI: 10.1109/MCOM.2016.7470933
- [6] HE Y X, WANG D W, HUANG F H, et al. A V2I and V2V collaboration framework to support emergency communications in ABS-aided Internet of vehicles [J]. *IEEE transactions on green communications and networking*, 2023, 7(4): 2038 – 2051. DOI: 10.1109/TGCN.2023.3245098
- [7] LIU T X, MIN S, LYU R L, et al. UAV assisted heterogeneous wireless networks: potentials and challenges [J]. *ZTE communications*, 2018, 16(2): 3 – 8. DOI: 10.3969/J.ISSN.1673-5188.2018.02.002
- [8] WANG P F, SONG W, SUN G, et al. Air-ground integrated low-energy federated learning for secure 6G communications [J]. *ZTE Communications*, 2022, 20(4): 32 – 40. DOI: 10.12142/ZTECOM.202204005
- [9] SHEN Y, OU P, CHEN F K, et al. Reconfigurable intelligent surface-assisted channel characteristics in 5G high-speed railway scenario [J]. *Journal of Beijing Jiaotong University*, 2023, 47(2): 23 – 35. DOI: 10.11860/j.issn.1673-0291.20220098
- [10] XU S Y, LYU J S. Maximizing UAV coverage efficiency based on retransmission in the Internet of Things [J]. *Journal of Beijing Jiaotong University*, 2023, 47(2): 58 – 66. DOI: 10.11860/j.issn.1673-0291.20220133
- [11] ALSAMHI S H, SHVETSOV A V, KUMAR S, et al. Computing in the sky: a survey on intelligent ubiquitous computing for UAV-assisted 6G networks and industry 4.0/5.0 [J]. *Drones*, 2022, 6(7): 177. DOI: 10.3390/drones6070177
- [12] CHENG X, HUANG Z W, BAI L. Channel nonstationarity and consistency for beyond 5G and 6G: a survey [J]. *IEEE communications surveys & tutorials*, 2022, 24(3): 1634 – 1669. DOI: 10.1109/COMST.2022.3184049
- [13] AN H, GUAN K, LI W B, et al. Measurement and ray-tracing for UAV air-to-air channel modeling [C]//*Proceedings of IEEE 5th International Conference on Electronic Information and Communication Technology (ICEICT)*. IEEE, 2022: 415 – 420. DOI: 10.1109/ICEICT55736.2022.9908966
- [14] WANG W J, SHI Y, MENG Z K, et al. A metasurface design method for dual wide band radar cross section reduction [J]. *Chinese journal of radio science*, 2021, 36(6): 887 – 895
- [15] DE QUEVEDO Á D, URZAIZ F I, MENOYO J G, et al. Drone detection with X-band ubiquitous radar [C]//*Proceedings of 19th International Radar Symposium (IRS)*. IEEE, 2018: 1 – 10. DOI: 10.23919/IRS.2018.8447942
- [16] SEDIVY P, NEMEC O. Drone RCS statistical behaviour [EB/OL]. (2021-11-07) [2023-04-16]. <https://www.sto.nato.int/publications/STO%20Meeting%20Proceedings/STO-MP-MSG-SET-183/MP-MSG-SET-183-04.pdf>
- [17] GUAY R, DROLET G, BRAY R J. Measurement and modelling of the dynamic radar cross-section of an unmanned aerial vehicle [J]. *IET radar, sonar & navigation*, 2017, 11(7): 1155 – 1160
- [18] EZUMA M, ANJINAPPA C K, SEMKIN V, et al. Comparative analysis of radar-cross-section-based UAV recognition techniques [J]. *IEEE sensors journal*, 2022, 22(18): 17932 – 17949. DOI: 10.1109/JSEN.2022.3194527
- [19] EZUMA M, ANJINAPPA C K, FUNDERBURK M, et al. Radar cross section based statistical recognition of UAVs at microwave frequencies [J]. *IEEE transactions on aerospace and electronic systems*, 2021, 58(1): 27 – 46. DOI: 10.1109/TAES.2021.3096875
- [20] SEMKIN V, YIN M S, HU Y Q, et al. Drone detection and classification based on radar cross section signatures [C]//*International Symposium on Antennas and Propagation (ISAP)*. IEEE, 2021: 223 – 224
- [21] SEMKIN V, HAARLA J, PAIRON T, et al. Analyzing radar cross section signatures of diverse drone models at mmWave frequencies [J]. *IEEE access*, 2020, 8: 48958 – 48969. DOI: 10.1109/ACCESS.2020.2979339
- [22] LIAO N W, QIAN P Z, CHEN Y, et al. A joint planning method for the number of UAVs and spectrum resource in perceptual missions [J]. *Chinese journal of radio science*, 2023, 38(5): 764 – 772. DOI: 10.12265/j.cjors.2022212
- [23] HE D P, AI B, GUAN K, et al. The design and applications of high-performance ray-tracing simulation platform for 5G and beyond wireless communications: a tutorial [J]. *IEEE communications surveys & tutorials*, 2018, 21(1): 10 – 27. DOI: 10.1109/COMST.2018.2865724.
- [24] LIN Y C, ZHONG Z D, GUAN K, et al. Channel characteristic of millimeter wave massive MIMO under train-to-infrastructure scenario based on ray-tracing method [J]. *Chinese journal of radio science*, 2017, 32(5): 595 – 601. DOI: 10.13443/j.cjors.2017080902
- [25] KNOTT E F, SCHAEFFER J F, TULLEY M T. *Radar cross section* [M]. Henderson, USA: SciTech Publishing, 2004
- [26] HE D P, GUAN K, AI B, et al. Channel measurement and ray-tracing simulation for 77 GHz automotive radar [J]. *IEEE transactions on intelligent transportation systems*, 2022, 24(7): 7746 – 7756. DOI: 10.1109/TITS.2022.3208008
- [27] HE D P, GUAN K, YAN D, et al. Physics and AI-based digital twin of

multi-spectrum propagation characteristics for communication and sensing in 6G and beyond [J]. IEEE journal on selected areas in communications, 2023, 41(11): 3461 - 3473. DOI: 10.1109/JSAC.2023.3310108

### Biographies

**AN Hao** received his BE degree in communication engineering from Beijing Information and Science Technology University, China in 2021. He is currently pursuing his PhD degree with the School of Electronic and Information Engineering, Beijing Jiaotong University, China. He received the Best Paper Award in ICEICT 2022. His current research interests include measurement and modeling of wireless propagation channels, UAV communications, and integrated sensing and communications.

**LIU Ting** received her BE degrees from both Beijing Jiaotong University, China and Lancaster University (with first-class honors), UK in 2021, in electronic and communication engineering. She is currently working toward her doctoral degree with the School of Electronic and Information Engineering, Beijing Jiaotong University. Her current research interests include radio propagation, deterministic channel modelling, and hybrid channel modelling for ISAC.

**HE Danping** (hedanping@bjtu.edu.cn) received her BE degree from Huazhong University of Science and Technology, China in 2008, MS degree from the Université Catholique de Louvain, Belgium and Politecnico di Torino, Italy in 2010, and PhD degree from Universidad Politécnica de Madrid, Spain in 2014. In 2012, she was a visiting scholar with Institut National de Recherche en Informatique et en Automatique, France. From 2014 to 2015, she was a research en-

gineer with Huawei Technologies. From 2016 to 2018, she was a postdoctoral researcher with the State Key Laboratory of Rail Traffic Control and Safety, Beijing Jiaotong University, China. She is currently with Beijing Jiaotong University as an associate professor. She has authored or coauthored more than 60 papers, three patents and one IEEE standard. Her research interests include radio propagation and channel modeling, ray tracing simulator development and wireless communication algorithm design. She is a member of the CA15104 Initiative, and was the recipient of five Best Paper Awards.

**MA Yihua** received his BE degree from Southeast University, China in 2015 and MS degree from Peking University, China in 2018. He has been with ZTE Corporation since 2018, where he is now an expert-level research engineer in the Department of Algorithm and a member of the State Key Laboratory of Mobile Network and Mobile Multimedia Technology, China. His main research interests include mMTC, joint communication and sensing, grant-free transmission, and massive MIMO.

**DOU Jianwu** received his PhD degree in robotic mechanism from Beijing University of Technology, China in 2001. From 2000 to 2014, he was the leader of the Wireless RRM Team, ZTE Corporation including 2G/3G/4G/WLAN and was in charge of developing the multi-RAT wireless system simulation platform. From 2012 to 2014, he was the product manager of ZTE iNES, a multi-cell/multi-UE hardware wireless channel emulator. From 2005 to 2017, he was the vice director of Wireless Algorithm Department of ZTE Corporation. His current research interests are B5G/6G channel modeling, new air-interface, unmanned aerial vehicles, non-terrestrial network research, THz, meta-materials and RIS. Dr. DOU received the Science and Technology Award (the 1st Level) in 2014/2015 and the Award for Chinese Outstanding Patented Invention in 2011 from China Institute of Communications and WIPO-SIPO, respectively.